Journal Pre-proof

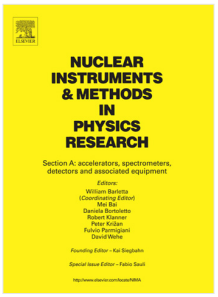

Nanoporosity imaging by positronium lifetime tomography

K. Dulski, E. Beyene, N. Chug, C. Curceanu, E. Czerwiński, M. Das, M. Gorgol, B. Jasińska, K. Kacprzak, Ł. Kapłon, G. Korcyl, T. Kozik, K. Kubat, D. Kumar, E. Lisowski, F. Lisowski, J. Mędrala-Sowa, S. Niedźwiecki, P. Pandey, S. Parzych, E. Perez del Rio, M. Rädler, S. Sharma, M. Skurzok, K. Tayefi, P. Tanty, E.Ł. Stępień, P. Moskal

PII: S0168-9002(26)00037-9
DOI: https://doi.org/10.1016/j.nima.2026.171311
Reference: NIMA 171311

To appear in: *Nuclear Inst. and Methods in Physics Research, A*

Received date : 14 August 2025
Revised date : 22 December 2025
Accepted date : 23 January 2026

Please cite this article as: K. Dulski, E. Beyene, N. Chug et al., Nanoporosity imaging by positronium lifetime tomography, *Nuclear Inst. and Methods in Physics Research, A* (2026), doi: https://doi.org/10.1016/j.nima.2026.171311.

Nanoporosity imaging by positronium lifetime tomography

K. Dulski[1,2,*], E. Beyene[1,2], N. Chug[1,2], C. Curceanu[3], E. Czerwiński[1,2], M. Das[1,2], M. Gorgol[4], B. Jasińska[4], K. Kacprzak[1,2], Ł. Kapłon[1,2], G. Korcyl[1,2], T. Kozik[1,2], K. Kubat[1,2], D. Kumar[1,2], E. Lisowski[5], F. Lisowski[5], J. Mędrala-Sowa[1,2], S. Niedźwiecki[1,2], P. Pandey[1,2], S. Parzych[1,2], E. Perez del Rio[1,2], M. Rädler[1,2], S. Sharma[1,2], M. Skurzok[1,2], K. Tayefi[1,2], P. Tanty[1,2], E. Ł. Stępień[1,2], and P. Moskal[1,2,*]

[1]Faculty of Physics, Astronomy and Applied Computer Science, Jagiellonian University, S. Łojasiewicza 11, 30-348 Krakow, Poland; [2]Centre for Theranostics, Jagiellonian University, Kopernika 40, 31-501 Krakow, Poland; [3]INFN, Laboratori Nazionali di Frascati, Via E. Fermi 40, 00044 Frascati, Italy; [4]Institute of Physics, Maria Curie-Skłodowska University, Radziszewskiego 10, 20-031 Lublin, Poland; [5]Cracow University of Technology, Warszawska 24, 31-864 Kraków, Poland; [*]corresponding author, e-mail: kamil.dulski@uj.edu.pl or p.moskal@uj.edu.pl

This manuscript was compiled on December 22, 2025

Positron Annihilation Lifetime Spectroscopy (PALS) is a well-established non-destructive technique used for nanostructural characterization of porous materials. It is based on the annihilation of a positron and an electron. Mean positron lifetime in the material depends on the free voids size and molecular environment, allowing the study of porosity and structural transitions in the nanometer scale. We have developed a novel method enabling spatially resolved PALS, thus providing tomography of nanostructural characterization of an extended object. Correlating space (position) and structural (lifetime) information brings new insight in materials studies, especially in the characterization of the purity and pore distribution. For the first time, a porosity image using stationary positron sources for the simultaneous measurement of the porous polymers XAD4, silica aerogel powder IC3100, and polyvinyl toluene scintillator PVT by the J-PET (Jagiellonian Positron Emission Tomography) system is demonstrated.

Positron, PALS, Nanoporosity imaging, Nanoporous materials

*

INTRODUCTION

The development of imaging techniques and the characterization of materials in three dimensions opens the possibility to study new structural relationships and differentiation of changes across distinct layers of a sample. The most common techniques, such as Focused Ion Beam (FIB), X-ray computed tomography (X-ray CT), Laser Scanning Confocal Microscopy (LSCM) and Transmission Electron Microscopy (TEM) provide high-resolution imaging of samples at the micro- and nanometer scales (1, 2). However, sample preparation in FIB, LSCM, and in TEM can often result in the alteration or destruction of the studied specimen(1). In addition, there are some limitations to the volume of the sample that can be imaged (up to $(10\ \mu m)^3$ for FIB (1, 2)) or requiring very thin samples (10 μm for TEM (3), 7 μm thick for LSCM (1)), the preparation of which is often very complicated and time-consuming. In contrast, X-ray CT allows one to measure samples in a wide range of sizes (2, 4). However, it allows only to characterize pores in the micrometer scale. Therefore, nanostructural information coming from the measurement of the mean positronium lifetime (7, 8) could become a complementary technique, allowing enhanced porosity imaging of the matter (9), although this would require greater control over the delivery of positrons to the sample (10, 11). Here we demonstrate a method of imaging of the nano-porosity in large objects (tens of cm) by a novel technique combining the Positron Annihilation Lifetime Spectroscopy (PALS) and Positron Emission Tomography (PET). The main novelty of the method lies in the determination of the annihilation location and the positron lifetime for each event separately, and to perform PALS analysis for each voxel of the reconstructed PET image.

PALS is a well-established technique that enables the study of porosity and phase transitions in matter such as porous silica, metals, compounds and semiconductors (7, 8, 12–20) and biological samples (21–24). The annihilation of electron and positron may proceed via formation of a quasi-stable two-body system - positronium (Ps) with a mass of 1.022 MeV/c^2. Positronium, depending on its total spin (S), can be formed in two states: para-positronium (p-Ps, $\mathbf{S} = 0$) or ortho-positronium (o-Ps, $\mathbf{S} = 1$). Due to the conservation of charge conjugation symmetry singlet state p-Ps annihilates with emission of even number of photons, unlike triplet state o-Ps which annihilates with emission of odd number of photons (25). An additional factor distinguishing the two states of positronium is the average time after which they annihilate (mean lifetime). In a vacuum, p-Ps annihilates with mean lifetime of 0.125 ns (27), in contrast to o-Ps which annihilates after mean lifetime of 142 ns (28). The mean lifetime of o-Ps decreases significantly in materials and depends on the material nano-structure (7, 8). In PALS the lifetime of a positron is usually extracted by using a specific isotope (e.g.^{22}Na) which, after β^+ decay, enters the excited state of the daughter nuclide, which then deexcites with emission of gamma quantum, hereinafter referred to as a deexcitation photon.

[*]To whom correspondence should be addressed. E-mail: kamil.dulski@uj.edu.pl or p.moskal@uj.edu.pl

Time difference between the emission of annihilation and deexcitation photon can be used as an estimate of the lifetime of the positron that annihilated.

The mean o-Ps lifetime is a sensitive probe to the structure and chemical environment in which it is located. The relationship between the mean lifetime of a positron and the size of free volumes (pores) is the basis of PALS (12–15). The shortening of the mean o-Ps lifetime can be translated into the radius of free volume using the Tao-Eldrup model (12, 13) or its extensions (14, 15), for inorganic matter measured in a vacuum. It was also found that in the presence of free radicals, the mean lifetime of o-Ps may be additionally shortened due to the o-Ps to p-Ps conversion processes (29, 30).

PET is used in medical diagnostics for imaging of the metabolism rate of radiopharmaceuticals in tissues of the living organism (31–36). In PET, radiopharmaceuticals are labeled with β^+ radionuclide, and photons emitted from the body due to the positron-electron annihilations are used to reconstruct an image of the annihilation density distribution which reflects the metabolic rate. Recently, the Jagiellonian PET group (J-PET), had reported the idea (37) and simulation-based feasibility study of combining PALS and PET techniques in the so-called positronium imaging (38–42). Additionally, the development of imaging reconstruction techniques specially adapted to positronium imaging allows obtaining image resolution comparable to those obtained in standard PET (43–48).

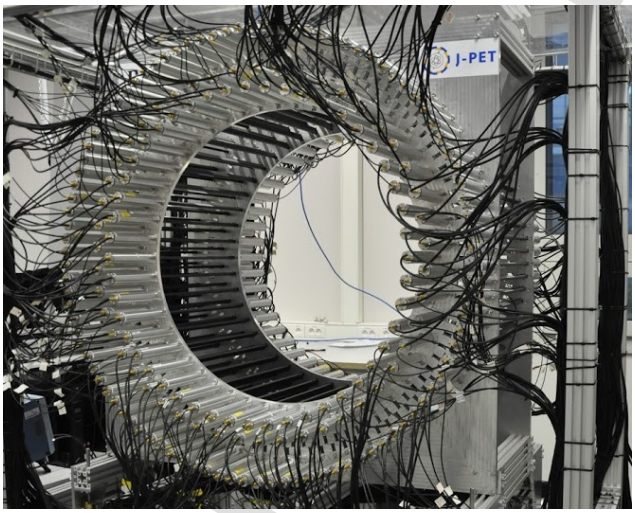

Fig. 1. Photograph of the J-PET detector constructed in the Jagiellonian University (51). 192 polymer scintillation strips with 50 cm length (black strips) are ordered in three concentric cylindrical layers with radius 42.5, 46.75 and 57.5 cm. Both ends of the scintillation strip is connected to the Hamamatsu R9800 vacuum photomultipliers (grey tubes) (49, 50). Light signal created in the scintillators are converted to electric signals by photomultipliers and then transferred to the data acquisition system, digitized (53) and acquired by the dedicated FPGA system (54).

In this work, mean o-Ps lifetime images will be demonstrated for three samples of different porosity - the porous polymers XAD4, the silica aerogel powder IC3100, and the polyvinyl toluene scintillator PVT. The samples were chosen solely to serve as reference materials with well-documented porosity distributions available in the literature. This allowed for a qualitative comparison between known characteristics and the spatially resolved positronium lifetime values obtained through image reconstruction, thereby demonstrating the potential of the proposed methodology. However, it should be noted that our measurements were performed under atmospheric conditions to demonstrate the imaging technique itself and not to present the results of tests on the materials themselves. It will be the first image of this type obtained for porous samples, which allows for the tomographic imaging of the free void size distributions in large extended objects. The designed positronium image reconstruction algorithm for the J-PET detector made it possible to obtain a resolution of several centimeters.

THE J-PET DETECTOR AND MEASUREMENT DETAILS

The J-PET (Jagiellonian Positron Emission Tomography) detector (Fig. 1) was constructed from long EJ-230 plastic scintillator strips (49–51). Dimensions of each strip are equal to $1.9 \times 0.7 \times 50$ cm^3. Scintillator strips in the detector are arranged in three concentric cylindrical layers (with radii 42.5, 46.75 and 57.5 cm) (49–51). The long strips and large radii of the layers allows to measure large samples, even up to $40 \times 40 \times 40$ cm^3. Light signals generated inside the scintillation strips are converted into electric signals by Hamamatsu R9800 vacuum photomultipliers (52) coupled to both ends of the strip.

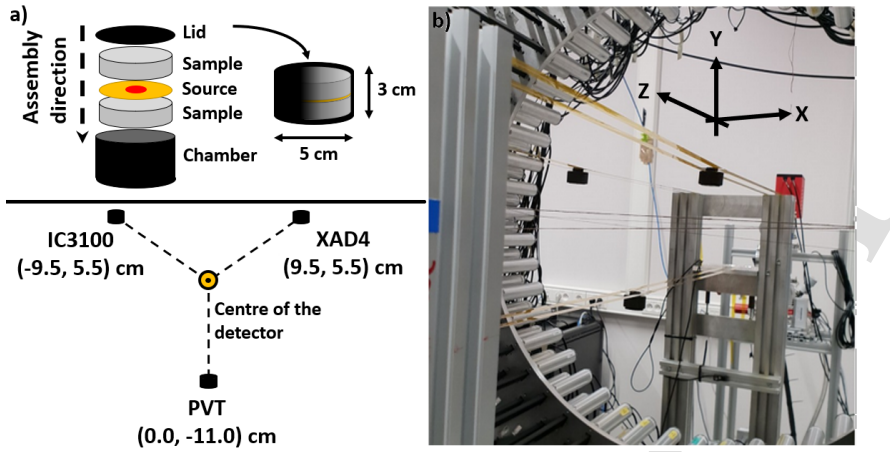

Fig. 2. (a) Scheme of the measurement setup and plastic chambers used in the measurement with three materials - IC3100, XAD4 and PVT. In the brackets positions in XY plane are given. In the axial direction (Z) the samples were placed in the middle of the scintillators in order to obtain highest detection efficiency. Each chamber was equidistant from the centre of the detector, hanged on Kapton foil scaffolding. (b) Photo of the setup inserted into the detector. Chambers were placed on a Kapton scaffolding.

Electric signals are sampled at four voltage thresholds and converted to the time stamps by front-end electronics (53). The data are acquired by a trigger-less system (54) and analyzed using dedicated *Framework* (42, 55). In the J-PET detector, time of the signal is estimated as the time on the lowest threshold with resolution of 350 ps at Full-width-at-half-maximum (FWHM), which corresponds to the spatial resolution of 5 cm (FWHM) (57), when position of positron-electron annihilation is reconstructed based on the time. It is worth noting that the spatial resolution value takes into account both the time resolution and the blurring resulting from the detector size. Next generation J-PET prototypes and development of new materials for better timing (58) allow for further improvement of spatial resolutions (33, 40, 59). The new J-PET prototypes should be also characterized by a higher sensitivity, therefore allowing an additional reduction of the measurement time (33, 40).

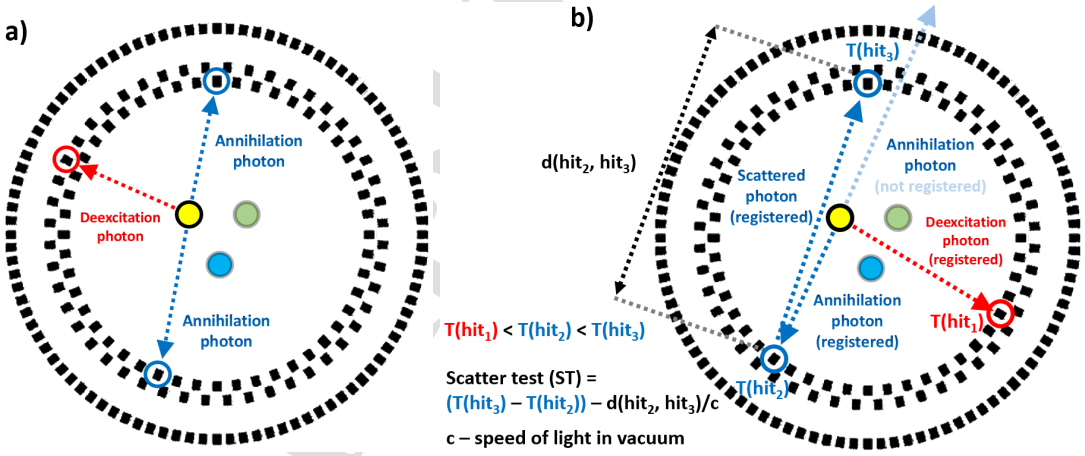

Fig. 3. (a) Measurement setup consisted of three samples (circles), each marked with different colour - IC3100 with yellow, XAD4 with green and PVT with blue, that were inserted to the J-PET detector (black rectangles). Example of the event used for the imaging and lifetime estimation coming from the sample marked as yellow - two annihilation photons (blue dashed arrows) and one deexcitation photon (red dashed arrow) registered in the J-PET detector. (b) Exemplary scheme of an event with the scattering of the annihilation photon. One of the annihilation photon scatters in the detection module and therefore it is registered due to a trigger-less system, and its scattering is also registered in the second module. In addition, the second annihilation photon is not registered. Such scatterings can be rejected by using scatter test defined in the figure.

A measurement with three materials (XAD4 powder (60), IC3100 powder (61) and PVT - scintillator (62)) that differ in mean lifetime of o-Ps (63) was conducted in order to check the ability of the J-PET detector to spatially characterize mean lifetime of positronium during a single measurement. The experimental setup is shown in Fig. 2. Three ^{22} Na radioactive sources (activity 0.24, 0.39 and 0.35 MBq used for XAD, IC3100 and PVT respectively) in thin Kapton foil were used as positron emitters. ^{22}Na nucleus during β^+ decay emits a positron with an energy of about 545 keV and transforms into the excited state of ^{22}Ne, which after about 4 ps emits a deexcitation photon with an energy of 1275 keV (64). Each source was surrounded by a different material and inserted into a plastic cylindrical chamber shown schematically in Fig. 2 a). To keep the same detection efficiency, each chamber was placed at the same distance from the center of the detector.

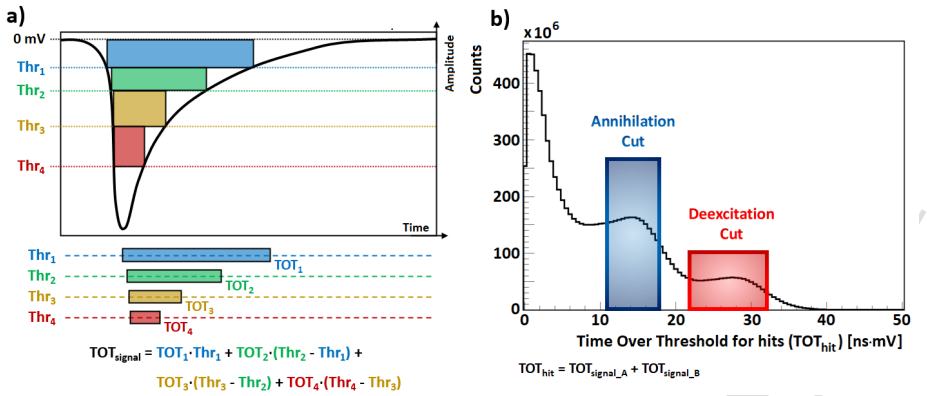

Fig. 4. (a) Pictorial scheme of the time-over-threshold (TOT) definition for the J-PET detector. TOT of the signal is a weighted sum of the TOTs for individual thresholds, with weights depending on the threshold value (Thr). (b) Hit TOT distribution. A single strip is connected to two photomultipliers (A and B) and the Hit TOT is defined as the sum of signal TOTs for both ends of the strip. Selection criteria for annihilation and deexcitation photons are marked with blue and red, respectively.

Conditions (temperature 21°C ± 0.5°C, pressure 997.7 ± 2 hPa, humidity 58.9 ± 7.5 %) were stable during the measurement. Fig. 3 a) indicates a cross section of the J-PET detector with the superimposed arrows depicting photons from the signal event: annihilations (blue) and deexcitation (red). For each registered photon a time and position of interaction is calculated. Position and time of annihilation photons interaction are used to reconstruct the annihilation position (51) while the time difference between emission of annihilation and deexcitation photons enables to calculate the positron lifetime for each registered event separately. Annihilation and deexcitation photons are disentangled based on the measurement of the time-over-threshold (TOT) of registered electric signals. Definition of TOT is presented graphically in Fig. 4 a). TOT scales with the photon energy as it was shown recently in the reference (56).

IMAGING AND LIFETIME ANALYSIS

The analysis of the data collected from the measurement was divided onto several steps: data selection, background reduction, annihilation position distribution reconstruction and PALS analysis for each voxel of the imaged objects. For the applied selection criteria and detector geometry, a comprehensive analysis of the possibilities of imaging positronium lifetimes (65, 66) was carried out based on simulations performed by dedicated simulation software in Geant4 (39, 40). The resulting positron lifetime distribution was decomposed by a dedicated software PALS Avalanche (67, 68).

DATA SELECTION. The first step was focused on the reconstruction of the signals, hits and events from the trigger-less data acquisition. A signal corresponds to eight timestamps measured at four threshold levels at the leading and trailing edges of the electric pulse from a single photomultiplier. The time of the signal is taken as the time on the lowest threshold. A pair of signals within 50 ns time window from photomultipliers connected to the same scintillator strip formed a hit. The time window is chosen to collect all photons coming from deexcitation, which, as seen in Fig. 4 b), generate TOT mainly in the range of 20-40 ns. A hit is defined as a reconstructed interaction point characterized by the time, position and TOT. A set of hits in 200 ns time window formed an event, which is four times the longest expected mean o-Ps lifetime for IC3100 - about 50 ns, allowing the collection of the vast majority of events originating from o-Ps decays regardless of the material. An example of the event that will allow the reconstruction of the annihilation position and positron lifetime estimation is schematically shown in Fig. 3 a). After reconstructing all of the events, further analysis was conducted on the event-by-event basis. For each hit in the event, the energy-equivalent TOT value was calculated (56). Definition of the TOT of the signal can be seen in Fig. 4 a). Based on the TOT value, a hit was assigned to one of the two categories:

$$\text{Annihilation hits where } 11 \leq \ \text{TOT}_{\text{hit}} \leq 18,$$

$$\text{Deexcitation hits where } 22 \leq \ \text{TOT}_{\text{hit}} \leq 32.$$

To establish a reference time (emission of a deexcitation photon) and estimate the lifetime of a positron, at least two annihilation and one additional deexcitation hit must be a part of the same event. The reconstructed position is assigned to an event (including the deexcitation hit from the event) based on the positions and times of the annihilation hits from that event. The simplest and most common case of an event with these characteristics was selected, which consisted of two annihilation hits along with one deexcitation hit. The distribution of hit TOT values with selection ranges superimposed for the two categories is shown in Fig. 4 b).

BACKGROUND REDUCTION. To reduce the impact of various background sources that can cause artifacts the final images, such as secondary scattering of photons in the detector (shown schematically in Fig. 3 b), cosmic rays, random coincidences and electronic noises, a set of selection criteria has been introduced. The selection criteria set consisted of:

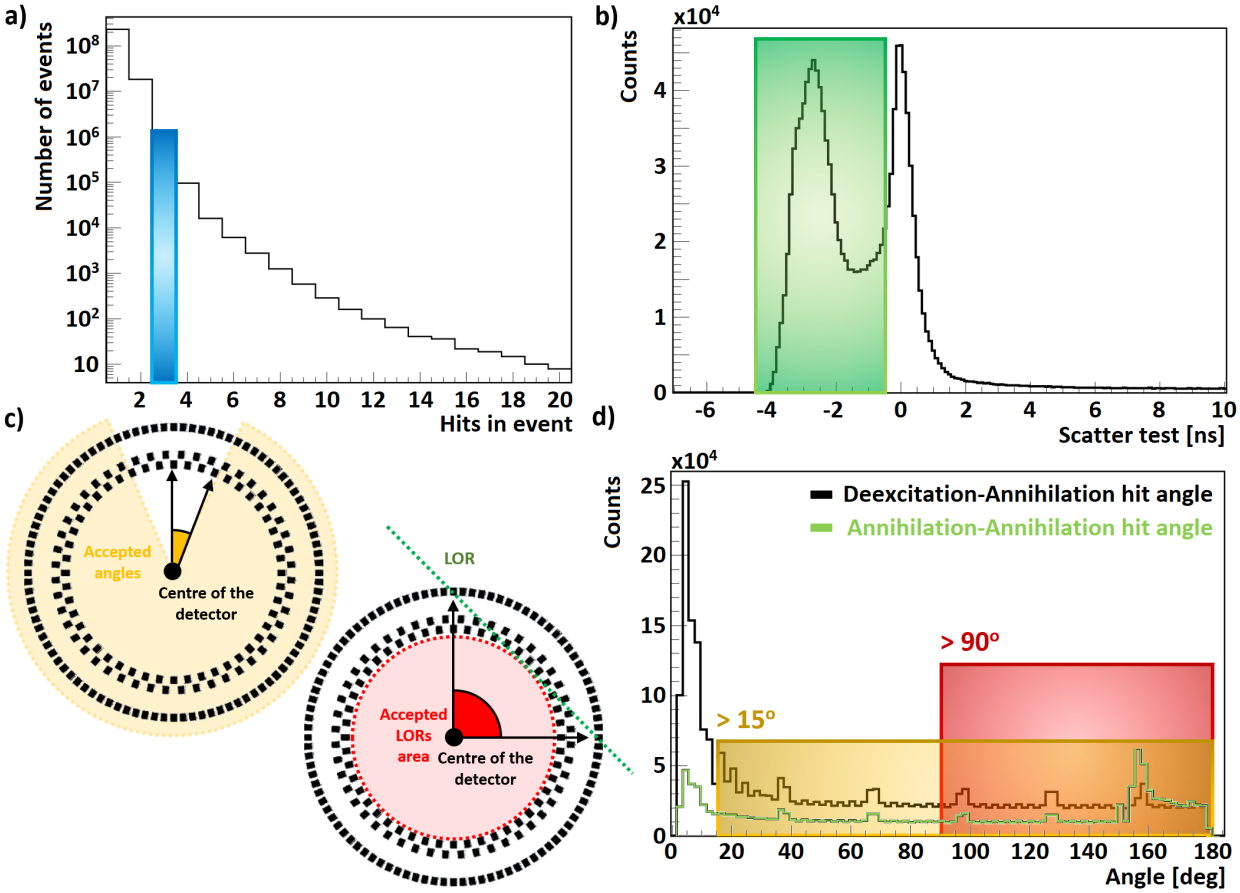

Fig. 5. (a) Multiplicity distribution of hits in event. Blue rectangular indicates which event multiplicity was selected for further analysis. Tail coming from multiplicity 4 to 20 shows the influence of multiple scatterings, the positron-electron decays on more photons, accidental coincidences, and cosmic rays. (b) Scatter test distribution for candidates for annihilation hits. One can see three structures, the first peak for negative values correspond to the true back-to-back pair with very small time differences, which exclude the possibility of scattering. The second peak around zero comes from the true scatterings in which time difference is comparable to the time a photon would need to travel between two scintillators. At last the long tail for positive values of the scatter test originates from the accidental coincidences and misidentification of the annihilation with the deexcitation hit or its scattering. Green area indicates range of acceptance of events. (c) Selected ranges of angles between any annihilation and deexcitation hits (orange) and between annihilation hits only (red) selected for further analysis. Angle between annihilation hits can be translated to the range of LORs, that are accepted. (d) Distribution of angles between two hits in an event previously categorized as both originating from annihilation (yellow), or one originating from annihilation and the other from deexcitation of a ^{22}Na nucleus (black), counted from the center. The stepped structure of the distribution comes from the geometry of the J-PET detector and the enhancement for some bins comes from inclusion of two scintillators within one bin every 30°, starting from 7.5° bin, which is the period of the first layer of scintillators. The peak near zero originates from the scatterings between neighbouring scintillators. Orange area indicates the acceptance range of the angle between deexcitation and annihilation hits, to reduce scatterings between neighbouring scintillators. Red area indicates the acceptance range of the angle between hits classified as annihilation candidates to ensure that annihilation took place inside the detector.

1. Multiplicity cut - to avoid ambiguity of proper selection of hits in event, number of hits in event (multiplicity) should be exactly three (where two of them should be categorized as annihilation, and the third one as deexcitation) as shown in Fig. 5 (a);

2. Scatter test - to reduce the misidentification of secondary scattered photon as the annihilation hit (Fig. 3 b), a scatter test (ST) was introduced as:

$$\mathrm{ST} = \Delta \mathrm{t}\left(hit_1, hit_2\right) - \frac{\mathrm{d}\left(hit_1, hit_2\right)}{\mathrm{c}}$$

where Δt is a time difference between registration of two hits, d is a distance between two hit positions, and c is the speed of light in vacuum. In case of the misidentification due to the scattering the value of ST is equal to zero. To avoid disturbing the positron lifetime distribution, which is based on a reference time of deexcitation hit, the scatter test was performed only for the hits that were assigned as annihilation hits. Cut-off for the test was selected as -0.5 ns ($\mathrm{ST} \leq -0.5$ ns) as shown in Fig. 5 (b);

3. Angular cuts - to additionally reduce scatterings between neighbouring scintillators, that could survive the previous condition, the minimal angle between any hits in event should be greater than 15°. Moreover, in order to further reduce contribution of scatterings, the angle between annihilation hits, measured from the center, was required to be greater than 90°. Angle cuts and the schemes of the geometries rejected by the used condition is shown in Fig. 5 (c and d).

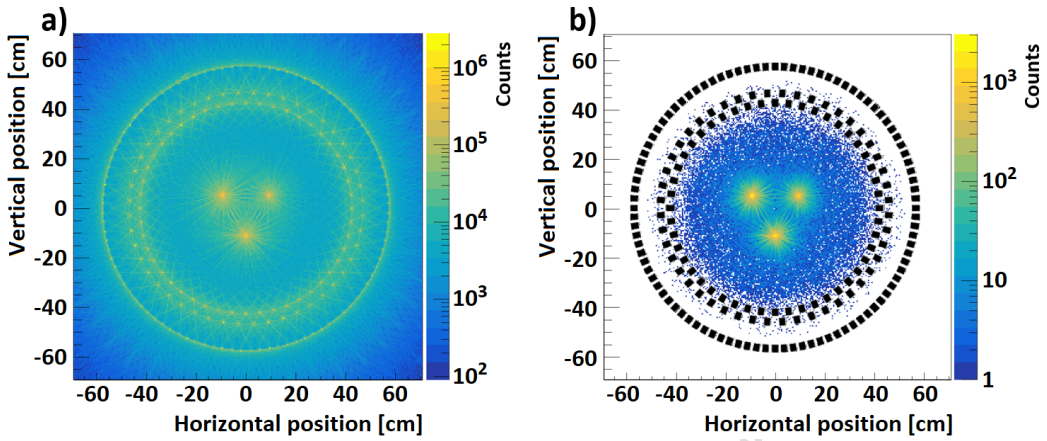

Fig. 6. (a) Distribution of all of the annihilation positions before applying selection criteria. The green circles covering the scintillator positions are from events in which both classified annihilation hits came from the scattering of a single photon, while other annihilation photon was not registered. (b) Distribution of the annihilation positions after applying selection criteria. To guide an eye black rectangles indicate positions of the scintillators. There are still some scatterings and accidental coincidences ($\approx 0.7\%$) that have survived the selection criteria used, visible between the black rectangles.

POSITION RECONSTRUCTION. At the last stage of the analysis, image is created from the events that have fulfilled the entire selection criteria. From selected events, the position of annihilation is estimated based on the position and time of registration of the annihilation hits (51):

$$\frac{\overrightarrow{\mathrm{P}\left(hit_1\right)}+\overrightarrow{\mathrm{P}\left(hit_2\right)}}{2}+\left(\mathrm{T}\left(hit_1\right)-\mathrm{T}\left(hit_2\right)\right)\times\ \mathrm{c}\ \times\widehat{P}_{1\to 2}, \qquad [1]$$

where P is a position of the hit, T is the time of the hit, c is the speed of light in vacuum and $\widehat{P}_{1\to 2}$ is a versor directed from the P(hit_1) to P(hit_2). A projection onto XY plane of the reconstructed annihilation points, forming an image of the β^+ activity distribution, before and after applying the selection criteria is shown in Fig. 6 a) and b). In the image one can clearly see the positions of each sample, with no clear distinction between different materials. The reconstructed annihilation rate should be proportional to the activity of the β^+ source. Which is confirmed by calculating the ratio of events in the image to the source activity (second row in Tab. 1).

POSITRONIUM LIFETIME IMAGING

POSITRON LIFETIME DISTRIBUTION. At each location in the activity image (voxel), one can determine the positron annihilation lifetime spectrum based on the reference time coming from the deexcitation photon. Positron lifetime for a single event can be estimated as (41):

$$\frac{\left|\mathrm{T}\left(hit_1^{Anni}\right)+\mathrm{T}\left(hit_2^{Anni}\right)\right|}{2}-\mathrm{T}\left(hit^{Deex}\right), \qquad [2]$$

where T is the time of a hit, hit_1^{Anni} and hit_2^{Anni} are the annihilation hits selected in a given event, and hit^{Deex} is the deexcitation hit in this event. The lifetime spectrum of positronium may be determined for each voxel of the annihilation rate image. As an example, Fig. 7 a) shows exemplary positron lifetime distribution for voxels inside the circles with radius of 2.5 cm around the center of the samples which contain most of the activity inside. The spectrum comprises contributions from annihilation of p-Ps, direct electron-positron annihilation, annihilation in the material surrounding the source, background from accidental coincidences, and the o-Ps components. The contribution from the long-lived o-Ps is clearly visible, especially in the spectrum of IC3100 material (Fig. 7 b) for which the spectrum approaches the accidental background level only at about 200 ns. During the fitting, the number of o-Ps components was set to two for XAD4 and IC3100 and one for PVT, which was consistent with the literature results and gave good fits measured by the adjusted R^2 value. Typically, the number of o-Ps components for a given sample indicates the presence of so many types of pores in the sample, differing in shape, size, or chemical composition

The results of the decomposition into different components of the lifetime of the positron by fitting each lifetime distribution of the positron from Fig. 7 a) are shown in Table 1, and the exemplary decomposed spectrum for the IC3100 is shown in Figs. 7 b) and c). Fitting was performed by PALS Avalanche software (67, 68). Contribution from the annihilations in Kapton foil that contained the ^{22}Na source, was fixed to the known values of 10% intensity and 0.374 ns mean lifetime (63). As the most sensitive structural probe is a o-Ps mean lifetime distribution, to stabilize fitting procedure, mean lifetime of the p-Ps was fixed to the theoretical value in vacuum amounting to 0.125 ns (27).

Results from the Table 1 indicate that, the differences of the o-Ps mean lifetime in the investigated materials are in the order of tens of nanoseconds. It is worth to notice, that the measurement was conducted in the atmospheric pressure, so due to the conversion processes, the obtained results differ from literature values (131.9 (0.3) ns for IC3100, 90.8 (1.2) ns for XAD4, 2.05 (04) ns for PVT)(62, 63), that were obtained from measurements in vacuum.

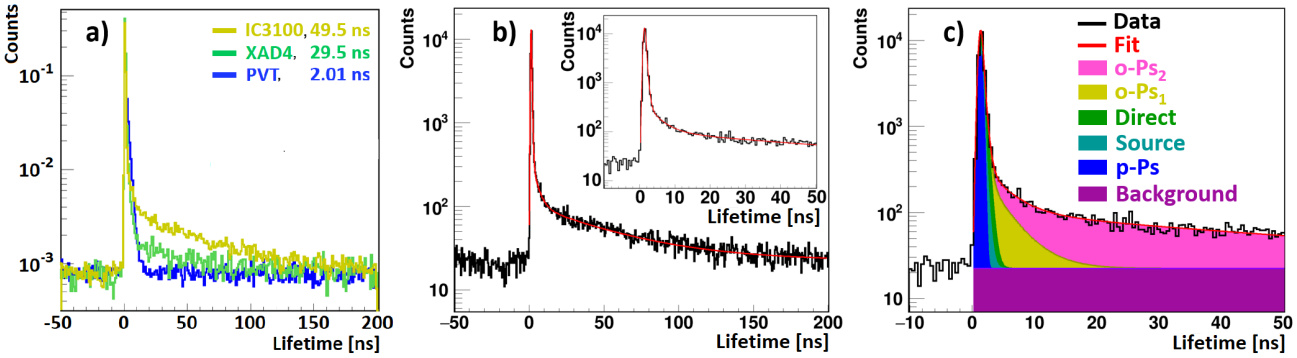

Fig. 7. (a) Positron lifetime distribution for each material used in the measurement. Distributions obtained from hits positioned inside three regions of interest are marked with appropriate colors. Distributions are normalized such that the accidental coincidences background is on the same level. Fitting each distribution resulted in obtaining mean o-Ps lifetime (longest component) for each sample - 49.5 ns for IC3100 (yellow), 29.6 ns for XAD4 (green) and 2.01 ns for PVT (blue). (b) Positron lifetime spectrum determined for the IC3100 sample. Superimposed red curve indicates the result of the fit. (c) Positron lifetime spectrum (as above). Superimposed histograms indicate in a cumulative way, contributions to the spectrum from o-Ps annihilations, direct annihilation, annihilation in the source, p-Ps annihilation and the background.

Table 1. Results from fitting positron annihilation lifetime spectra for three materials used for the measurement - IC3100, XAD4, PVT. Contribution of the annihilation in the Kapton foil was excluded from the total intensity of the positron annihilation.

Parameter name	IC3100	XAD4	PVT
Total number of counts	53542	35313	52408
Activity of the source [MBq]	0.393	0.238	0.345
p-Ps mean lifetime (fixed parameter) [ns]	0.125	0.125	0.125
p-Ps intensity [%]	21.98 (61)	13.41 (98)	22.47 (55)
direct annihilation mean lifetime [ns]	0.385 (06)	0.383 (06)	0.408 (11)
direct annihilation intensity [%]	45.18 (28)	65.44 (28)	31.91 (51)
o-Ps mean lifetime 1 component [ns]	3.39 (21)	1.64 (05)	2.01 (02)
o-Ps intensity 1 component [%]	6.97 (07)	15.89 (01)	45.61 (51)
o-Ps mean lifetime 2 component [ns]	49.5 (1.2)	29.5 (2.8)	-
o-Ps intensity 2 component [%]	25.86 (34)	5.25 (29)	-
Reduced Chi Squared	0.9682	1.0778	1.1527
Voxel-wise mean o-Ps lifetime for the longest component [ns]	51.96 (91)	30.05 (63)	2.40 (58)
Voxel-wise pore radius [nm]	1.94 (05)	1.27 (04)	0.29 (06)

LIFETIME IMAGING AND NANOPOROSITY MAP. For the next step, an image voxel was established to the size of $1 \times 1 \times 6$ cm^3, from which the distribution of positron lifetimes was collected from. The voxel size in the axial direction was larger due to the poorer resolution in this dimension (standard deviation (σ) 0.72 cm (1.69 cm in FWHM) for the horizontal and vertical directions and 3 cm (7.05 cm in FWHM) for the axial direction) (51). This made it possible to obtain about several thousand counts per voxel near the sources. Resulting positronium lifetime image for defined voxels is shown in Fig. 8 a). The distribution of pore size in the imaged materials can be estimated based on the mean lifetime of the o-Ps components from the Tao-Eldrup model (12, 13) and its modifications (7, 8, 15). The relation between the mean o-Ps lifetime and the mean radius of the free voids is shown in Fig. 8 b). It is worth emphasizing that the impact of various processes influencing the shortening of the mean o-Ps lifetime, such as pick-off and ortho-para conversion, was not distinguished.
To increase the contrast only the highest intensity voxels are shown, where the total number of counts is at least 5% of the maximum total number of counts for a single voxel. It is clearly visible that there is a difference in the pore size between three regions corresponding to different materials used in the measurement.

CONCLUSIONS

Combining information from the positronium decay, the position of annihilation, and the lifetime of positronium, gives the possibility of a more complex analysis of materials. The simultaneous spatial and structural characteristics of materials can be used in the study of structural changes in sample, diffusion inside the sample, and many others. This may be of particular interest in the field of characterizing the porosity of matter in space, where techniques such as FIB, X-ray CT, LSCM, and

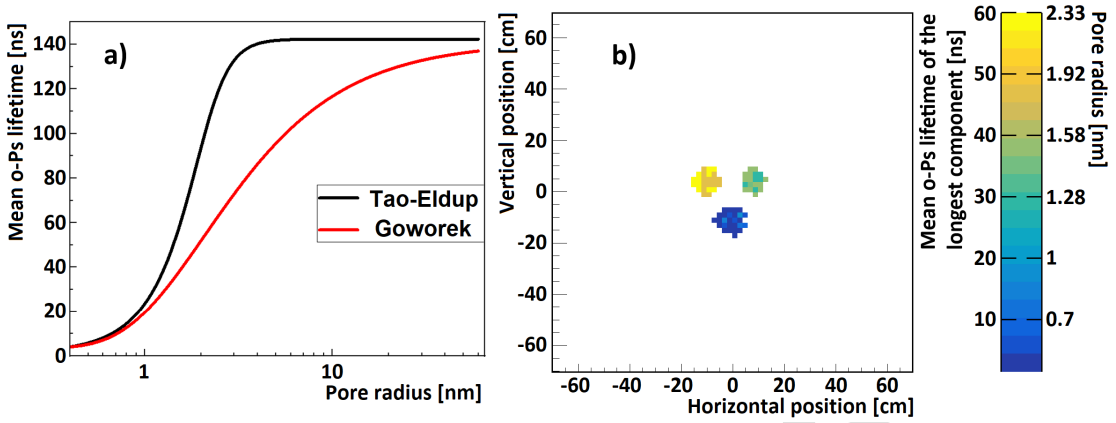

Fig. 8. (a) Mean o-Ps lifetime of the longest o-Ps component as a function of the mean pore radius, following Tao-Eldrup and Goworek model (13, 15). (b) Positron lifetime map constructed from the mean ortho-positronium lifetime of the longest component estimates for voxels where the total number of counts were at least 5% of the maximum total number of counts for a single voxel (67 voxels visible). There is a visible difference between three areas which are representing materials that differ in mean positron lifetime, according to Table 1 (top left - IC3100, top right - XAD4, bottom - PVT). Using Goworek model mean o-Ps lifetime scale was recalculated to the pores radius.

TEM are currently used. This is particularly true given that information on pico- and nanometer-sized defects, which can be collected using positron lifetime spectroscopy, could be a complementary technique to those mentioned above.

Measurement with three materials (IC3100, XAD4, PVT) differing in mean positronium lifetime (131.9 ns vs 90.8 ns vs 2.05 ns, measured in vacuum) and consequently the pore radius (22 nm vs 3.8 nm vs 0.3 nm) was carried out using the J-PET detector. The choice of porous materials used in this study was not motivated by their specific application but only served as reference distributions for the distributions after reconstruction. Dedicated data selection was used to reduce various background sources such as scatterings, cosmic rays, and electronic noise. Analysis of the positron annihilation lifetime distribution sampled in three different areas showed the J-PET detector's ability to accurately estimate the mean positron lifetime of different components (p-Ps, o-Ps, and direct annihilation) in each area separately. It should be noted that these components differ in their applications: o-Ps is sensitive to defects ranging in size from 0.5 to even 10 nm; direct annihilation samples very well very small defects < 0.5 nm; and p-Ps is particularly sensitive to the presence of some heavier elements in the sample (69).

The presented results highlight J-PET as the first multiphoton PET system with the ability to obtain a porosity image based on positron annihilation. Further development of detectors in the context of time resolution (70) and detection resolution (71) as well as significant improvement in sensitivity based on Total-Body projects (72–75) may also lead to an improvement in the quality of positronium images, including even millimeter resolution, where increased efficiency will also significantly reduce measurement time. It is also worth mentioning that intensive efforts are currently underway to design and optimize image reconstruction methods and link them to the lifetime distribution (43–48), which will help both improve spatial resolution and estimate average lifetimes in single voxels.

Furthermore, the motivation to continue this research may also be to extend the capabilities of PET, which allows much earlier diagnosis, which can improve the effectiveness of cancer therapy. It is also worth noting that positron annihilation may become a sensitive probe also in fundamental research, especially in the test of discrete symmetry violation (76–86), quantum entanglement (85, 87–89) and forbidden decays (90, 91).

AUTHOR CONTRIBUTION

The experiment was conducted using the Jagiellonian Positron Emission Tomograph (J-PET). The J- PET scanner, the techniques of the experiment and this study was conceived by P.M. The preparation of the experimental setup and samples was done by K.D. The data analysis was conducted by K.D. Signal selection criteria were developed by P.M. and K.D. and applied by K.D. Authors: K.D., E.B., N.C., C.C., E.C., M.D., M.G., B.J., K.Kacprzak, Ł.K., G.K., T.K., K. Kubat, D.K., E.L., F.L., J.M-S., S.N., P.P., S.P., E.PdR., M.R.m S.S., M.S. E.Ł.S., K.T., P.T. and P.M participated in the construction, commissioning, and operation of the experimental setup, as well as in the data-taking campaign and data interpretation. K.D. under the supervision of P.M. monitored the whole data taking campaign. M.G. and B.J. designed and constructed the positronium production chamber. G.K. and S.N. optimized the working parameters of the detector. K.D. and K. Kacprzak, took part in developing the J-PET analysis and simulation framework. K.D., M.S., K.K. and E.PdR. performed timing calibration of the detector. E.C. developed and operated short- and long-term data archiving systems and the computer center of J-PET. S.S. established relation between energy loss and TOT and dependence of detection efficiency on energy deposition. P.M. managed the whole project and secured the main financing. The results were interpreted by K.D. and P.M.. The manuscript was prepared by K.D. and P.M. and was then edited and approved by all authors.

ACKNOWLEDGMENT

The authors would like to acknowledge the technical support from A. Heczko, M. Kajetanowicz, and W. Migdał. The authors are also grateful to the J-PET members for their editorial remarks on the earlier version of the manuscript. We acknowledge the support provided by the National Science Centre of Poland through grants no. 2021/42/A/ST2/00423 (P.M.), 2021/43/B/ST2/02150 (P.M.), 2022/47/I/NZ7/03112 (E.Ł.S) and 2021/41/N/ST2/03950 (K.D.); the Ministry of Education and Science through grants no. SPUB/SP/490528/2021 (P.M.), IAL/SP/596235/2023 (P.M.); as well as the SciMat and qLife Priority Research Area budgets under the programme Excellence Initiative - Research University at the Jagiellonian University (P.M.).

REFERENCES

1. M.H.N. Yio, M.J. Mac, H.S. Wong, N.R. Buenfeld 3D imaging of cement-based materials at submicron resolution by combining laser scanning confocal microscopy with serial sectioning. *Journal of Microscopy* ***258*** 2015, p. 151
2. L. Salvo, M. Suéry, A. Marmottant, N. Limodin, D. Bernard 3D imaging in material science: Application of X-ray tomography. *Comptes Rendus Physique* ***11*** 2010, p. 641
3. S. Sadamatsu, M. Tanaka, K. Higashida, S. Matsumura Transmission electron microscopy of bulk specimens over 10 µm in thickness. *Ultramicroscopy* ***162*** 2016, p. 10
4. M. Madadi, A.C. Jones, C.H. Arns, M.A. Knackstedt 3D Imaging and Simulation of Elastic Properties of Porous Materials. *IEEE: Computing in Science and Engineering* ***11*** 2009, p. 65
5. M. Iwaniszyn, K. Sindera, A. Gancarczyk, B. Leszczyński, M. Korpyś, M. Suwak, A. Kołodziej, P.J. Jodłowski Characterization of Fluid Flow and Heat Transfer of Expanded Metal Meshes for Catalytic Processes. *Energies* ***15*** 2022, p. 8437
6. D. Panek, M. Szczepanek, B. Leszczyński, P. Moskal, E. Stępień Comparison of Lugol's solution and Fe3O4 nanoparticles as contrast agents for tumor spheroid imaging using microcomputed tomography. *Bio-Algorithms and Med-Systems* ***18*** 2022, p. 158
7. D.W. Gidley, H.G Peng, R.S. Vallery Positron Annihilation as a Method to Characterize Porous Materials. *Annual Review of Materials Research* ***36*** 2006, p. 49
8. C. Zahasky, S.M. Benson Micro-Positron Emission Tomography for Measuring Sub-core Scale Single and Multiphase Transport Parameters in Porous Media. *Advances in Water Resources* ***115*** 2018, p. 1
9. R.H. Howell, T.E. Cowan, J. Hartley, P. Sterne, B. Brown Positron beam lifetime spectroscopy of atomic scale defect distributions in bulk and microscopic volumes. *Applied Surface Science* ***116*** 1997, p. 7
10. T.L. Audet, A. Alejo, L. Calvin, M.H. Cunningham, G.R. Frazer, G. Nersisyan, M. Phipps, J.R. Warwick, G. Sarri Ultrashort, MeV-scale laser-plasma positron source for positron annihilation lifetime spectroscopy. *Phys. Rev. Accel. Beams* ***24*** 2021, p. 073402
11. A. Wagner, W. Anwand, M. Butterling, T.E. Cowan, F. Fiedler, F. Fritz, M. Kempe, R. Krause-Rehberg Positron-Annihilation Lifetime Spectroscopy using Electron Bremsstrahlung. *J. Phys.: Conf. Ser.* ***618*** 2015, p. 012042
12. J.S. Tao Positronium annihilation in molecular substances. *J. Chem. Phys.* ***56*** 1972, p. 5499
13. M. Eldrup, D. Lightbody, J.N. Sherwood The temperature dependence of positron lifetimes in solid pivalic acid. *Chem. Phys.* ***63*** 1981, p. 51
14. K. Wada, T. Hyodo A simple shape-free model for pore-size estimation with positron annihilation lifetime spectroscopy. *Conf. Series* ***443*** 2013, p. 012003
15. T. Goworek, K. Ciesielski, B. Jasińska, J. Wawryszczuk Positronium states in the pores of silica gel. *Chem. Phys. Lett.* ***272*** 1997, p. 91
16. H. Uhlig, G. Adouane, C. Bluhm, S. Zieger, R. Krause-Rehberg, D. Enke Positron-Annihilation-Lifetime-Spectroscopy (PALS)for the characterization of bimodal silica-gel synthesized by pseudomorphic transformation. *J. Porous Mater.* ***23*** 2016, p. 139
17. J. Sun, D. W. Gidley, T. L. Dull, W.E. Frieze, A.F. Yee, E.T. Ryan, S. Lin, J. Wetzel Probing diffusion barrier integrity on porous silica low-k thin filmsusing positron annihilation lifetime spectroscopy. *J. Appl. Phys.* ***89*** 2001, p. 5138
18. E.M. Hassan, B.A.A. Balboul, M.A. Abdel-Rahman Probing the Phase Transition in Nanocrystalline TiO2 Powders by Positron Lifetime (PAL) Technique. *Defects Diff. Forum* ***319*** 2011, p. 151
19. F. Hori, T. Yano, Y. Yokoyama, Y. Akeno, T.J. Konno Free volume change in crystallization process of Zr–Cu–Al metallic glass studied by positron annihilation techniques. *J. Alloys Comp.* ***434*** 2007, p. 207
20. O. Shpotyuk, R. Golovchak, A. Ingram, V. Boyko, L. Shpotyuk Comparative study of extended free-volume defects in As- and Ge-based glassy semiconductors: theoretical prediction and experimental probing with PAL technique. *Phys. Status Solidi C* ***10*** 2013, p. 117
21. T. Ahn, D.W. Gidley, A.W. Thornton, A.G. Wong-Foy, B.G. Orr, K.M. Kozløff, M.M. Banaszak Holl Hierarchical Nature of Nanoscale Porosity in Bone Revealed by Positron Annihilation Lifetime Spectroscopy. *ACS Nano* ***15*** 2021, p. 4321
22. H. Karimi, P. Moskal, A. Żak, E.Ł. Stępień 3D melanoma spheroid model for the development of positronium biomarkers. *Scientific Reports* ***13*** 2023, p. 7648
23. P. Moskal, E. Kubicz, G. Grudzień, E. Czerwiński, K. Dulski, B. Leszczyński, S. Niedźwiecki, E.Ł. Stępień Developing a novel positronium biomarker for cardiac myxoma imaging. *EJNMMI Phys.* ***10*** 2023, 22
24. S. Moyo, P. Moskal, E.Ł. Stępień Feasibility study of positronium application for blood clots structural characteristics. *Bio-Algorithms and Med-Systems* ***18*** 2022, p. 163
25. S.D. Bass, S. Mariazzi, P. Moskal, E. Stępień Colloquium: Positronium physics and biomedical applications. *Rev. Mod. Phys.* ***95*** 2023, 021002
26. D.G. Cassidy Experimental progress in positronium laser physics. *Eur. Phys. J. D* ***53*** 2018, p. 72
27. A.H. Al-Ramadhan and D.W. Gidley New precision measurement of the decay rate of singlet positronium. *Phys. Rev. Lett.* ***72*** 1994, p. 1632
28. Y. Kataoka, S. Asai and T. Kobayashi First test of O (α^2) correction of the orthopositronium decay rate. *Phys. Lett. B* ***671*** 2009, p. 219
29. P.S. Stepanov, F.A. Selim, S.V. Stepanov, A.V. Bokov, O.V. Ilyukhina, G. Duplatre, V.M. Byakov Interaction of positronium with dissolved oxygen in liquids. *Phys. Chem. Chem. Phys. 22*, 2020, p. 5123
30. K. Shibuya, H. Saito, F. Nishikido, M. Takahashi, T. Yamaya Oxygen sensing ability of positronium atom for tumor hypoxia imaging. *Communications Physics* ***3***, 2020, 173
31. A. Alavi, T.J. Werner, E.Ł. Stępień, P. Moskal Unparalleled and revolutionary impact of PET imaging on research and day to day practice of medicine. *Bio-Algorithms and Med-Systems* ***17***, 2021, 203
32. P. Moskal, E. Ł. Stępień Positronium as a biomarker of hypoxia. *Bio-Algorithms and Med-Systems* ***17*** 2021, p. 311
33. P. Moskal. E.Ł. Stępień Prospects and clinical perspectives of total-body PET imaging using plastic scintillators. *PET Clin.* ***15*** 2020, p. 439
34. J.P. Schmall, J.S. Karp, A. Alavi The Potential Role of Total Body PET Imaging in Assessment of Atherosclerosis. *PET Clin.* ***14*** 2019, p. 245
35. M.L. McKenney-Drake, M.C. Moghbel, K. Paydary, M. Alloosh, S. Houshmand, S. Moe, A. Salavati, J.M. Sturek, P.R. Territo, C. Weaver, T.J. Werner, P.F. Høilund-Carlsen, M. Sturek, A. Alavi ^{18}F-NaF and ^{18}F-FDG as molecular probes in the evaluation of atherosclerosis . *EJNMMI* ***45*** 2018, p. 2190
36. S. Vandenberghe, P. Moskal, J.S. Karp State of the art in total body PET. *EJNMMI Phys.* ***7*** 2020, p. 35
37. P. Moskal Positronium Imaging. *2019 IEEE Nuclear Science Symposium and Medical Imaging Conference (NSS/MIC)* 2019
38. P. Moskal, B. Jasińska, E.Ł. Stępień, S.D. Bass Positronium in medicine and biology. *Nature Reviews Physics* ***1*** 2019, p. 527
39. P. Moskal, D. Kisielewska, C. Curceanu, E. Czerwiński, K. Dulski, A. Gajos, M. Gorgol, B. Hiesmayr, B. Jasińska, K. Kacprzak, Ł. Kapłon, G. Korcyl, P. Kowalski, W. Krzemień, T. Kozik, E. Kubicz, M. Mohammed, Sz. Niedźwiecki, M. Pałka, M. Pawlik-Niedźwiecka, L. Raczyński, J. Raj, S. Sharma, Shivani, R.Y. Shopa, M. Silarski, M. Skurzok, E. Stępień, W. Wiślicki, B. Zgardzińska Feasibility study of the positronium imaging with the J-PET tomograph. *Phys. Med. Biol.* ***64*** 2019, p. 055017
40. P. Moskal, D. Kisielewska, Z. Bura, C. Chhokar, C. Curceanu, E. Czerwiński, M. Dadgar, K. Dulski, J. Gajewski, A. Gajos, M. Gorgol, R. Del Grande, B. C. Hiesmayr, B. Jasińska, K. Kacprzak, A. Kamińska, Ł. Kapłon, H. Karimi, G. Korcyl, P. Kowalski, N. Krawczyk, W. Krzemień, T. Kozik, E. Kubicz, P. Małczak, M. Mohammed, Sz. Niedźwiecki, M. Pałka, M. Pawlik-Niedźwiecka, M. Pędziwiatr, L. Raczyński, J. Raj, A. Ruciński, S. Sharma, Shivani, R. Y. Shopa, M. Silarski, M. Skurzok, E. Ł. Stępień, S. Vandenberghe, W. Wiślicki, B. Zgardzińska Performance assessment of the 2gamma positronium imaging with the total-body PET scanners. *EJNMMI Phys.* ***7*** 2020, p. 44
41. P. Moskal, K. Dulski, N. Chug, C. Curceanu, E. Czerwiński, M. Dadgar, J. Gajewski, A. Gajos, G. Grudzień, B.C. Hiesmayr, K. Kacprzak, Ł. Kapłon, H. Karimi, K. Klimaszewski, G. Korcyl, P. Kowalski, T. Kozik, N. Krawczyk, W. Krzemień, E. Kubicz, P. Małczak, S. Niedźwiecki, M. Pawlik-Niedźwiecka, M. Pędziwiatr, L. Raczyński, J. Raj, A. Ruciński, S. Sharma, Shivani, R.Y. Shopa, M. Silarski, M. Skurzok, E.Ł. Stępień, M. Szczepanek, F. Tayefi, W. Wiślicki Positronium imaging with the novel multiphoton PET scanner. *Science Advances* ***7*** 2021, p. eabh4394
42. P. Moskal, J. Baran, S. Bass, J. Choiński, N. Chug, C. Curceanu, E. Czerwiński, M. Dadgar, M. Das, K. Dulski, K.V. Eliyan, K. Fronczewska, A. Gajos, K. Kacprzak, M. Kajetanowicz, T. Kaplanoglu, Ł. Kapłon, K. Klimaszewski, M. Kobylecka, G. Korcyl, T. Kozik, W. Krzemień, K. Kubat, D. Kumar, J. Kunikowska, J. Mączewska, W. Migdał, G. Moskal, W. Mryka, S. Niedźwiecki, S. Parzych, E. Perez del Rio, L. Raczyński, S. Sharma, Shivani, R.Y. Shopa, M. Silarski, M. Skurzok, F. Tayefi, K. Tayefi, P. Tanty, W. Wiślicki, L. Królicki, E. Ł. Stępień First positronium image of the human brain in vivo. *Science Advances* ***10*** 2024, p. adp2890
43. R.Y. Shopa, K. Dulski Multi-photon time-of-flight MLEM application for the positronium imaging in J-PET. Bio-Algorithms and Med-Systems **18**, 2022 p. 135

44. J. Qi, B. Huang Positronium Lifetime Image Reconstruction for TOF PET imaging in J-PET. IEEE Transactions on Medical Imaging **41**, 2022, p. 2848
45. H.H. Huang, Z. Zhu, S. Booppasiri, Z. Chen, S. Pang, C.M. Kao A statistical reconstruction algorithm for positronium lifetime imaging using time-of-flight positron emission tomography. Front. Phys. **12** 2024, p. 1429344
46. B. Huang, T. Li, G, Arino-Estrada, K. Dulski, R.Y. Shopa, P. Moskal, E. Stępień, J. Qi SPLIT: Statistical Positronium Lifetime Image reconstruction via time-Thresholding. IEEE Transactions on Medical Imaging **43**, 2024, p. 2148
47. R.Y. Shopa, K. Dulski Positronium imaging in J-PET with an iterative activity reconstruction and a multistage fitting algorithm Bio-Algorithms and Med-Systems **19**, 2023, p. 54
48. Z. Chen, L. An, C.M. Kao, H.H. Huang The properties of the positronium lifetime image reconstruction based on maximum likelihood estimation Bio-Algorithms and Med-Systems **19**, 2023, p. 1
49. P. Moskal, Sz. Niedźwiecki, T. Bednarski, E. Czerwiński, Ł. Kapłon, E. Kubicz, I. Moskal, M. Pawlik-Niedźwiecka, N.G. Sharma, M. Silarski, M. Zieliński, N. Zoń, P. Białas, A. Gajos, A. Kochanowski, G. Korcyl, J. Kowal, P. Kowalski, T. Kozik, W. Krzemień, M. Molenda, M. Pałka, L. Raczyński, Z. Rudy, P. Salabura, A. Słomski, J. Smyrski, A. Strzelecki, A. Wieczorek, W. Wiślicki Test of a single module of the J-PET scanner based on plastic scintillators. *Nucl. Instr. and Meth. A* ***764*** 2014, p. 317
50. P. Moskal, N. Zoń, T. Bednarski, P. Białas, E. Czerwiński, A. Gajos, D. Kamińska, Ł. Kapłon, A. Kochanowski, G. Korcyl, J. Kowal, P. Kowalski, T. Kozik, W. Krzemień, E. Kubicz, Sz. Niedźwiecki, M. Pałka, L. Raczyński, Z. Rudy, O. Rundel, P. Salabura, N.G. Sharma, M. Silarski, A. Słomski, J. Smyrski, A. Strzelecki, A. Wieczorek, W. Wiślicki, M. Zieliński A novel method for the line-of-response and time-of-flight reconstruction in TOF-PET detectors based on a library of synchronized model signals. *Nuclear Inst. and Methods in Physics Research A* ***775*** 2015, p. 54
51. S. Niedźwiecki, P. Białas, C. Curceanu, E. Czerwiński, K. Dulski, A. Gajos, B. Głowacz, M. Gorgol, B.C. Hiesmayr, B. Jasińska, Ł. Kapłon, D. Kisielewska-Kamińska, G. Korcyl, P. Kowalski, T. Kozik, N. Krawczyk, W. Krzemień, E. Kubicz, M. Mohammed, M. Pawlik-Niedźwiecka, M. Pałka, L. Raczyński, Z. Rudy, N.G. Sharma, S. Sharma, R.Y. Shopa, M. Silarski, M. Skurzok, A. Wieczorek, W. Wiślicki, B. Zgardzińska, M. Zieliński, P. Moskal J-PET: A New Technology for the Whole-body PET Imaging. *Acta Phys. Pol. B* ***48*** 2017, p. 1567
52. http://hamamatsu.com, Photomultiplier tube R9800, last entered: July 6th, 2025
53. M. Pałka, P. Strzempek, G. Korcyl, T. Bednarski, Sz. Niedźwiecki, P. Białas, E. Czerwiński, K. Dulski, A. Gajos, B. Głowacz, M. Gorgol, B. Jasińska, D. Kamińska, M.Kajetanowicz, P. Kowalski, T. Kozik, W. Krzemień, E. Kubicz, M. Mohhamed, L. Raczyński, Z. Rudy, O. Rundel, P. Salabura, N.G. Sharma, M. Silarski, J. Smyrski, A. Strzelecki, A. Wieczorek, W. Wiślicki, M. Zieliński, B. Zgardzińska, P. Moskal Multichannel FPGA based MVT system for high precision time (20 ps RMS) and charge measurement. *JINST* ***12*** 2017, p. P08001
54. G. Korcyl, P. Białas, C. Curceanu, E. Czerwiński, K. Dulski, B. Flak, A. Gajos, B. Głowacz, M. Gorgol, B. C. Hiesmayr, B. Jasińska, K. Kacprzak, M. Kajetanowicz, D. Kisielewska, P. Kowalski, T. Kozik, N. Krawczyk, W. Krzemień, E. Kubicz, M. Mohammed, Sz. Niedźwiecki, M. Pawlik- Niedźwiecka, M. Pałka, L. Raczyński, P. Rajda, Z. Rudy, P. Salabura, N. G. Sharma, S. Sharma, R. Y. Shopa, M. Skurzok, M. Silarski, P. Strzempek, A. Wieczorek, W. Wiślicki, R. Zaleski, B. Zgardzińska, M. Zieliński, P. Moskal Evaluation of Single-Chip, Real-Time Tomographic Data Processing on FPGA - SoC Devices. *IEEE Transactions On Medical Imaging* ***37*** 2018, p. 2526
55. P. Moskal, E. Czerwiński, J. Raj, S. D. Bass, E. Beyene, N. Chug, A. Coussat, C. Curceanu, M. Dadgar, M. Das, K. Dulski, A. Gajos, M. Gorgol, B. C. Hiesmayr, B. Jasińska, K. Kacprzak, T. Kaplanoglu, Ł. Kapłon, K. Klimaszewski, P. Konieczka, G. Korcyl, T. Kozik, W. Krzemień, D. Kumar, S. Moyo, W. Mryka, S. Niedźwiecki, S. Parzych, E. Pérez del Río, L. Raczyński, S. Sharma, S. Choudhary, R. Y. Shopa, M. Silarski, M. Skurzok, E. Ł. Stępień, P. Tanty, F. T. Ardebili, K. T. Ardebili, K. V. Eliyan, W. Wiślicki Discrete symmetries tested at 10^{-4} precision using linear polarization of photons from positronium annihilations. *Nature Communications* ***15*** 2024, p. 78
56. S. Sharma, J. Chhokar, C. Curceanu, E. Czerwinski, M. Dadgar, K. Dulski, J. Gajewski, A. Gajos, M. Gorgol, N. Gupta-Sharma, R. Del Grande, B. C. Hiesmayr, B. Jasinska, K. Kacprzak, L. Kaplon, H. Karimi, D. Kisielewska, K. Klimaszewski, G. Korcyl, P. Kowalski, T. Kozik, N. Krawczyk, W. Krzemien, E. Kubicz, M. Mohammed, Sz. Niedzwiecki, M. Palka, M. Pawlik-Niedzwiecka, L. Raczynski, J. Raj, A. Rucinski, Shivani, R. Y. Shopa, M. Silarski, M. Skurzok, E. L. Stepien, W. Wislicki, B. Zgardzinska, P. Moskal Estimating relationship between the Time Over Threshold and energy loss by photons in plastic scintillators used in the J-PET scanner. *EJNMMI Phys.* ***7*** 2020, p. 39
57. D. Kamińska, A. Gajos, E. Czerwiński, D. Alfs, T. Bednarski, P. Białas, C. Curceanu, K. Dulski, B. Głowacz, N. Gupta-Sharma, M. Gorgol, B. C. Hiesmayr, B. Jasińska, G. Korcyl, P. Kowalski, W. Krzemień, N. Krawczyk, E. Kubicz, M. Mohammed, Sz. Niedźwiecki, M. Pawlik-Niedźwiecka, L. Raczyński, Z. Rudy, M. Silarski, A. Wieczorek, W. Wiślicki, B. Zgardzińska, M. Zieliński, P. Moskal A feasibility study of ortho-positronium decays measurement with the J-PET scanner based on plastic scintillators. *Eur. Phys. J. C* ***76*** 2016, p. 445
58. P. Lecoq, C. Morel, J. O Prior, D. Visvikis, S. Gundacker, E. Auffray, P. Križan, R.M. Turtos, D. Thers, E. Charbon, J. Varela, C. de La Taille, A. Rivetti, D. Breton, J. Pratte, J. Nuyts, S. Surti, S. Vandenberghe, P. Marsden, K. Parodi, J.M. Benlloch, M. Benoit Roadmap toward the 10 ps time-of-flight PET challenge. *Phys. Med. Biol.* ***65*** 2020, p. 21RM01
59. S. Vanderberghe, P. Moskal, J. Karp State of the art in total body PET. *EJNMMI Phys.* ***7*** 2020, p. 35
60. https://www.sigmaaldrich.com, CAS Number 37380-42-0, last entered: July 6th, 2025
61. https://www.cabotcorp.com, CAS Number 102262-30-6, last entered: July 6th, 2025
62. A. Wieczorek, K. Dulski, Sz. Niedźwiecki, D. Alfs, P. Białas, C. Curceanu, E. Czerwiński, A. Danel, A. Gajos, B. Głowacz, M. Gorgol, B. Hiesmayr, B. Jasińska, K. Kacprzak, D. Kamińska, Ł. Kapłon, A. Kochanowski, G. Korcyl, P. Kowalski, T. Kozik, W. Krzemień, E. Kubicz, M. Kucharek, M. Mohammed, M. Pawlik-Niedźwiecka, M. Pałka, L. Raczyński, Z. Rudy, O. Rundel, N. G. Sharma, M. Silarski, T. Uchacz, W. Wiślicki, B. Zgardzińska, M. Zieliński, P. Moskal Novel scintillating material 2-(4-styrylphenyl)benzoxazole for the fully digital and MRI compatible J-PET tomograph based on plastic scintillators. *PLoS ONE* ***12*** 2017, p. e0186728
63. B. Jasińska, M. Gorgol, M. Wiertel, R. Zaleski, D. Alfs, T. Bednarski, P. Białas, E. Czerwiński, K. Dulski, A. Gajos B. Głowacz, D. Kamińska, Ł. Kapłon, G. Korcyl, P. Kowalski, T. Kozik, W. Krzemień, E. Kubicz, M. Mohammed, Sz. Niedźwiecki, M. Pałka, L. Raczyński, Z. Rudy, O. Rundel, N.G. Sharma, M. Silarski, A. Słomski, A. Strzelecki, A. Wieczorek, W. Wiślicki, B. Zgardzińska, M. Zieliński, P. Moskal Determination of the 3gamma Fraction from Positron Annihilation in Mesoporous Materials for Symmetry Violation Experiment with J-PET Scanner. *Acta Phys. Pol. B* ***47*** 2016, p. 453
64. M. Das, W. Mryka, E.Y. Beyene, S. Parzych, S. Sharma, E. Stępień, P. Moskal Estimating the efficiency and purity for detecting annihilation and prompt photons for positronium imaging with J-PET using toy Monte Carlo simulation. *Bio-Algorithms and Med-Systems* ***19*** 2023, p. 87
65. K. Dulski, C. Curceanu, E. Czerwiński, A. Gajos, M. Gorgol, N. Gupta-Sharma, B. C. Hiesmayr, B. Jasińska, K. Kacprzak, Ł. Kapłon, D. Kisielewska, K. Klimaszewski, G. Korcyl, P. Kowalski, N. Krawczyk, W. Krzemień, T. Kozik, E. Kubicz, M. Mohammed, Sz. Niedźwiecki, M. Pałka, M. Pawlik-Niedźwiecka, L. Raczyński, J. Raj, K. Rakoczy, Z. Rudy, S. Sharma, Shivani, R. Y. Shopa, M. Silarski, M. Skurzok, W. Wiślicki, B. Zgardzińska, P. Moskal Commissioning of the J-PET detector in view of the positron annihilation lifetime spectroscopy. *Hyperfine Interact* ***18*** 2019, p. 239
66. K. Dulski, S.D. Bass, J. Chhokar, N. Chug, C. Curceanu, E. Czerwiński, M. Dagdar, J. Gajewski, A. Gajos, M. Gorgol, R. Del Grande, B.C. Hiesmayr, B. Jasińska, K. Kacprzak, Ł. Kapłon, H. Karimi, D. Kisielewska, K. Klimaszewski, P. Kopka, G. Korcyl, P. Kowalski, T. Kozik, N. Krawczyk, W. Krzemień, E. Kubicz, P. Małczak, M. Mohammed, Sz. Niedźwiecki, M. Pałka, M. Pawlik-Niedźwiecka, M. Pędziwiatr, L. Raczyński, J. Raj, A. Ruciński, S. Sharma, Shivani, R.Y. Shopa, M. Silarski, M. Skurzok, E.Ł. Stępień, F. Tayefi, W. Wiślicki, B. Zgardzińska, P. Moskal The J-PET detector—a tool for precision studies of ortho-positronium decays. *Nucl. Instrum. Meth. A* ***1008*** 2021, p. 165452
67. K. Dulski, B. Zgardzińska, P. Białas, C. Curceanu, E. Czerwiński, A. Gajos, B. Głowacz, M. Gorgol, B.C. Hiesmayr, B. Jasińska, D. Kisielewska-Kamińska, G. Korcyl, P. Kowalski, T. Kozik, N. Krawczyk, W. Krzemień, E. Kubicz, M. Mohammed, M. Pawlik-Niedźwiecka, S. Niedźwiecki, M. Pałka, L. Raczyński, J. Raj, Z. Rudy, N.G. Sharma, S. Sharma, Shivani, R.Y. Shopa, M. Silarski, M. Skurzok, A. Wieczorek, W. Wiślicki, M. Zieliński, P. Moskal Analysis procedure of the positronium lifetime spectra for the J-PET detector. *Acta Phys. Pol. A* ***132*** 2017, p. 1637
68. K. Dulski PALS Avalanche - A New PAL Spectra Analysis Software. *Acta. Phys. Pol. A* ***137*** 2020, p. 167
69. Y. Kobayashi, K. Sato, M. Yamawaki, K. Michishio, T. Oka, and M. Washio Energy dissipation of para-positronium in polymers and silica glass. *App. Phys. Exp.* ***15*** 2022, p. 076001
70. P. Lecoq, C. Morel, J.O. Prior Roadmap toward the 10 ps time-of-flight PET challenge. *Phys. Med. Biol.* ***65*** 2020, p. 21RM01
71. J. Smyrski, D. Alfs, T. Bednarski, P. Białas, E. Czerwiński, K. Dulski, A. Gajos, B. Głowacz, N. Gupta-Sharma, M. Gorgol, B. Jasińska, M. Kajetanowicz, D. Kamińska, G. Korcyl, P. Kowalski, W. Krzemień, N. Krawczyk, E. Kubicz, M. Mohammed, Sz. Niedźwiecki, M. Pawlik-Niedźwiecka, L. Raczyński, Z. Rudy, P. Salabura, M. Silarski, A. Strzelecki, A. Wieczorek, W. Wiślicki, J. Wojnarska, B. Zgardzińska, M. Zieliński, P. Moskal Measurement of gamma quantum interaction point in plastic scintillator with WLS strips. *Nucl. Instrum. Meth. A* ***851*** 2017, p. 39
72. P. Moskal, E.Ł. Stępień Perspectives on translation of positronium imaging into clinics. *Front. Phys.* ***10*** 2022, p. 969806
73. P. Moskal, P. Kowalski, R.Y. Shopa, L. Raczyński, J. Baran, N. Chug, C. Curceanu, E. Czerwiński, M. Dadgar, K. Dulski, A. Gajos, B.C. Hiesmayr, K. Kacprzak, Ł. Kapłon, D. Kisielewska, K. Klimaszewski, P. Kopka, G. Korcyl, N. Krawczyk, W. Krzemień, E. Kubicz, Sz. Niedźwiecki, Sz. Parzych, J. Raj, S. Sharma, S. Shivani, E. Stępień, F. Tayefi, W. Wiślicki Simulating NEMA characteristics of the modular total-body J-PET scanner - an economic total-body PET from plastic scintillators. *Phys. Med. Biol.* ***66*** 2021, p. 175015
74. F. Tayefi Ardebili, S. Niedźwiecki, P. Moskal Evaluation of Modular J-PET sensitivity. *Bio-Algorithms and Med-Systems* ***19*** 2023, p. 132
75. F. Tayefi Ardebili, P. Moskal Assessing the Spatial Resolution of the Modular J-PET Scanner using the Maximum-Likelihood Expectation-Maximization (MLEM) algorithm. *Bio-Algorithms and Med-Systems* ***20*** 2024, p. 1
76. A.P. Mills, S. Berko Search for C Nonconservation in Electron-Positron Annihilation. *Phys. Rev. Lett.* ***18*** 1967, p. 420
77. J. Yang, M. Chiba, R. Hamatsu, T. Hirose, T. Matsumoto, J. Yu Four-photon decay of orthopositronium: A test of charge-conjugation invariance. *Phys. Rev. A* ***54*** 1996, p. 1952
78. P.A. Vetter, S.J. Freedman Branching-ratio measurements of multiphoton decays of positronium. *Phys. Rev. A* ***66*** 2002, p. 052505
79. T. Yamazaki, T. Namba, S. Asai, T. Kobayashi Search for CP Violation in Positronium Decay. *Phys. Rev. Lett.* ***104*** 2010, p. 083401 Erratum: [Phys. Rev. Lett. **120** (2018) p. 239902]
80. M. Skalsey, J. Van House First test of CP invariance in the decay of positronium. *Phys. Rev. Lett.* ***67*** 1991, p. 1993
81. B.K. Arbic, S. Hatamian, M. Skalsey, J. Van House, W. Zheng Angular-correlation test of CPT in polarized positronium. *Phys. Rev. A* ***37*** 1988, p. 3189
82. P.A. Vetter, S.J. Freedman Search for CPT-Odd Decays of Positronium. *Phys. Rev. Lett.* ***91*** 2003, p. 263401
83. S.D. Bass QED and Fundamental Symmetries in Positronium Decays. *Acta Phys. Pol. B* ***50*** 2019, p. 7
84. A. Gajos Sensitivity of discrete symmetry tests in the positronium system with the J-PET detector. *Symmetry* ***12*** 2020, p. 1268
85. P. Moskal, A. Gajos, M. Mohammed, J. Chhokar, N. Chug, C. Curceanu, E. Czerwiński, M. Dadgar, K. Dulski, M. Gorgol, J. Goworek, B. Hiesmayr, B. Jasińska, K. Kacprzak, Ł. Kapłon, H. Karimi, D. Kisielewska, K. Klimaszewski, G. Korcyl, P. Kowalski, N. Krawczyk, W. Krzemień, T. Kozik, E. Kubicz, S. Niedźwiecki, S. Parzych, M. Pawlik-Niedźwiecka, L. Raczyński, J. Raj, S. Sharma, S. Choudhary, R. Shopa, A. Sienkiewicz, M. Silarski, M. Skurzok, E. Stepien, F. Tayefi, W. Wiślicki Testing CPT symmetry in ortho-positronium decays with positronium annihilation tomography. *Nature*

Communications ***12*** 2021, p. 5658
86. P. Moskal, D. Kumar, S. Sharma, E.Y. Beyene, N. Chug, A. Coussat, C. Curceanu, E. Czerwinski, M. Das, K. Dulski, M. Gorgol, B. Jasinska, K. Kacprzak, T. Kaplanoglu, L. Kaplon, K. Klimaszewski, T. Kozik, E. Lisowski, F. Lisowski, W. Mryka, S. Niedzwiecki, S. Parzych, E.P. del Rio, L. Raczynski, M. Radler, R.Y. Shopa, M. Skurzok, E. L. Stepien, P. Tanty, K. Tayefi Ardebili, K. Valsan Eliyan, W. Wislicki Non-maximal entanglement of photons from positron-electron annihilation demonstrated using a novel plastic PET scanner. *Science Advances* ***11***, 2025, p. eads3046
87. M. Nowakowski, D.B. Fierro Three Photon Entanglement from Ortho-Positronium Revisited. *Acta Phys. Polon. B* ***48*** 2017, p. 1955
88. B.C. Hiesmayr, P. Moskal Genuine Multipartite Entanglement in the 3-Photon Decay of Positronium. *Scientific Reports* ***7*** 2017, p. 15349
89. B.C. Hiesmayr, P. Moskal Witnessing Entanglement In Compton Scattering Processes Via Mutually Unbiased Bases. *Scientific Reports* ***9*** 2019, p. 8166
90. P. Tanty, E. Perez del Rio, P. Moskal Towards Studies of Rare Decays of Positronium with J-PET. *Acta Phys. Pol. B Proc. Suppl.* ***17*** 2024, p. 1
91. C. Vigo, L. Gerchow, B. Radics, M. Raaijmakers, A. Rubbia, P. Crivelli New Bounds from Positronium Decays on Massless Mirror Dark Photons. *Phys. Rev. Lett.* ***124*** 2020, p. 101803

Declaration of interests

☒ The authors declare that they have no known competing financial interests or personal relationships that could have appeared to influence the work reported in this paper.

☐ The authors declare the following financial interests/personal relationships which may be considered as potential competing interests: